Chemical Engineering Journal 248 (2014) 307–314

Contents lists available at ScienceDirect

Chemical Engineering Journal

journal homepage: www.elsevier.com/locate/cej

Facile fabrication of AuNPs/PANI/HNTs nanostructures for high-performance electrochemical sensors towards hydrogen peroxide

Pan Wang [b], Mingliang Du [a,b,*], Ming Zhang [a,b], Han Zhu [b], Shiyong Bao [b], Meiling Zou [b], Tingting Yang [b]

[a] Key Laboratory of Advanced Textile Materials and Manufacturing Technology, Zhejiang Sci-Tech University, Ministry of Education, Hangzhou 310018, PR China
[b] Department of Materials Engineering, College of Materials and Textile, Zhejiang Sci-Tech University, Hangzhou 310018, PR China

HIGHLIGHTS

- H_2O_2 detection biosensor using AuNPs/PANI/HNTs nanostructures was fabricated.
- *In situ* polymerization and reduction were employed.
- The biosensor exhibited high electrochemical performance.

ARTICLE INFO

Article history:
Received 10 January 2014
Received in revised form 7 March 2014
Accepted 12 March 2014
Available online 22 March 2014

Keywords:
Electrochemical sensors
Hydrogen peroxide
Polyaniline
Halloysite nanotubes
Gold nanoparticles

ABSTRACT

Here we proposed a facile strategy to synthesize multi-layered gold nanoparticles/polyaniline/halloysite nanotubes (AuNPs/PANI/HNTs) nanostructures used for electrochemical sensors. The PANI/HNTs were firstly obtained by making use of the *in situ* polymerization as well as employing the thioglycollic acid (TA) as the dopant, thereafter, Au ions were anchored to TA and then reduced by PANI. Field emission scanning electron microscopy (FE-SEM) and transmission electron microscopy (TEM) observations implied that a large amount of uniform AuNPs were immobilized on the PANI/HNTs. The as-prepared AuNPs/PANI/HNTs nanostructures were also characterized by Fourier transform infrared spectroscopy (FTIR), X-ray diffraction (XRD) and X-ray photoelectron spectroscopy (XPS), and the results confirmed the successful synthesis of AuNPs/PANI/HNTs nanostructures and explained the reactions in depth as well. Further investigations suggested that the AuNPs/PANI/HNTs nanostructures with well-separated AuNPs exhibited high electrochemical performance as sensors to detect hydrogen peroxide (H_2O_2).

1. Introduction

Electrochemical sensors have been drawing tremendous attention due to their great promise in a wide range of fields, such as industry and environmental monitoring, food inspection and medical diagnosis, since the initial development of glucose enzyme electrodes by Lyons and Clark in 1962 [1–3]. Recent years, with the increasingly serious environmental problems and peoples' close concerning to health, concentrated efforts have been focused on the detection of H_2O_2, considering its extensive applications in various fields such as biological, environmental, clinical, and food analysis [4], leading to an upsurge of interests to explore various H_2O_2 detectors. Recently, we synthesized AgNPs/(PVA/PEI) nanofibers and found that the nanofibers could be used as high electrochemical efficiency and durability for H_2O_2 electrochemical sensors [5]. Feng et al. have synthesized graphene/polyaniline composite film to detect H_2O_2 and the electrochemical sensor showed a good linear response over a manifold range of concentrations [6]. Apparently, multi-layered nanostructured materials have been extensively used as sensing materials, attributing to their high surface-to-volume ratios, high porosity and low cross-section.

Most recently, as far as representative conducting polymers, polyaniline has caught the eyes of researchers, considering its wide applications in actuators, gas sensors, electrochemical capacitors and memory devices [7,8]. In order to facilitate the electron transfer, metal nanoparticles have been widely employed to enhance electrocatalytic activity [9]. Therefore, metal nanoparticles combined with polyaniline have demonstrated functionality in a variety of fields [10]. Meanwhile, one of the important factors in

* Corresponding author at: Key Laboratory of Advanced Textile Materials and Manufacturing Technology, Zhejiang Sci-Tech University, Ministry of Education, Hangzhou 310018, PR China. Tel./fax: +86 571 86843255.
E-mail address: du@zstu.edu.cn (M. Du).

http://dx.doi.org/10.1016/j.cej.2014.03.044
1385-8947/

optimizing the properties of their applications is the stable and uniform size of the metal nanoparticles. Highly dispersed gold nanoparticles (AuNPs) have been discovered to be exceptionally active for a number of chemical reactions, such as oxidation and reduction [10,11]. However, the mechanical properties and long-term stability of the AuNPs/PANI remain a significant issue which deserves our attention and further exploration.

Halloysite nanotubes (HNTs, $Al_2Si_2O_5(OH)_4{\cdot}nH_2O$), an abundant deposited natural silicate resource with nanotubular structures, are easily obtainable and much cheaper, which could be collected from many parts of our country [12,13]. HNTs, a naturally occurred silicate with good chemical stability and large specific surface area, possess hollow structures with Al—OH groups in the internal surface and Si—OH groups on the external surface, making them easy to functionalize and perfect to be used as substrates. Recent years, HNTs were selected as reliable substrates in many scopes, such as, the organization of noble metal nanoparticles and many other materials with lower mechanical stability [14]. Inspired by their specific structure and wide applications, we also chose HNTs as dependent substrates to support our AuNPs/PANI nanofibers.

In the present investigation, we prepared PANI/HNTs nanostructures through a simple one-step *in situ* polymerization by using HNTs as templates and aniline as reactant. Additionally, we also introduced TA to dope the PANI and act as stabilizers as well to synthesis uniform and monodisperse AuNPs. Consequently, the AuNPs/PANI/HNTs were acquired. In another aspect, a series of characterizations were employed to detect and confirm the samples. The electrochemical performance of the as-obtained nanocomposites was also investigated in detail, and according to our results, the sensors based on the nanostructured AuNPs/PANI/HNTs composites exhibit high sensitivity towards H_2O_2.

2. Experimental section

2.1. Chemicals and materials

The HNTs were obtained from Hubei Province, China. Aniline (C_6H_7N, 99.9%), hydroquinone (HQ), H_2O_2 (30 wt%), horseradish peroxidase (HRP, RZ ~ 3, activity $\geqslant$250 units mg^{-1}), and thioglycollic acid ($C_2H_4O_2S$, TA, 98%) were supplied by Aladdin Chemistry Co., Ltd. Ammonium persulfate ($(NH_4)_2S_2O_8$, APS, 98%), glucose and ammonium hydroxide ($NH_3{\cdot}H_2O$, 27%) were acquired from Hangzhou Gaojing Fine Chemical Industry, and aniline was distilled under reduced pressure. Hydrochloric acid (HCl, 36%) was bought from Shanghai Three-eagles Chemical Reagent Co., Ltd. Chloroautic acid ($HAuCl_4{\cdot}4H_2O$, 99.9%) was collected from Shanghai Civi Chemical Technology Co., Ltd. Deionized water (DIW, 18.2 MΩ) was used for all solution preparations. All chemicals were analytical grade.

2.2. The fabrication of AuNPs/PANI/HNTs nanostructures

The PANI/HNTs nanostructures were synthesized by the one-step *in situ* polymerization of aniline in the presence of HNTs. A description of the synthesis method is given as follows. A solution of 75 mL of 1 M HCl containing 150 mg of HNTs was stirred and sonicated at room temperature for 1 h, successively. Then, 0.75 mL of aniline monomer was added to the above suspension and then was stirred for 1 h. After that, 0.45 g of APS dissolved in 2 mL of 1 M HCl solution was added into to the reaction mixture drop by drop slowly. When the suspension turned to dark green, the polymerization of aniline occurred. The solutions were kept at room temperature and left at rest to polymerize for 6 h. Followed by an excess of $NH_3{\cdot}H_2O$ (0.1 M) was used for dedoping and 3.5 mL of TA (1.0 M) was employed as a dopant. Then the PANI/HNTs nanostructures were collected using a centrifuge (at 12,000 rpm for 20 min) after being washed two times with DIW and alcohol and then dried under vacuum at 60 °C for 24 h.

The AuNPs were deposited onto the PANI/HNTs nanostructures *via* the reduction of Au ions. Typically, 20 mg of PANI/HNTs nanostructures were dispersed in 20 mL DIW by vigorous stirring for 2 h, then 1.44 mL of fresh prepared $HAuCl_4{\cdot}4H_2O$ (10 mM) was dropped into the suspensions. Several hours later, the AuNPs/PANI/HNTs nanostructures were obtained through the process of centrifuging, washing and drying, as described above.

2.3. The electrochemical measurement of AuNPs/PANI/HNTs nanostructures

The electrochemical experiments were conducted with a CHI660E workstation (Shanghai Chenhua, Shanghai). A three-electrode cell was employed for electrochemical evaluation in the PBS (pH = 6.8), where the Pt wire and a saturated Ag/AgCl electrode were used as the counter and reference electrodes, respectively. In the meantime, the HRP/(AuNPs/PANI/HNTs)/GCE was used as the working electrode, and the pure HNTs and the blank GCE were also selected as controls. Prior to the surface coating, the GC electrode was polished carefully with 1.0, 0.3, and 0.05 μm alumina powder and rinsed with DIW, followed by sonication in acetone and ethanol, successively. Appropriate amount of AuNPs/PANI/HNTs nanostructures and pure HNTs were mixed with Nafion (0.2%), respectively, and then were coated on the surface of the GCE. After that, the electrodes were allowed to dry under nitrogen and the PBS was also purged with nitrogen for 1 h prior to each experiment, so as to keep over the solution from oxygen.

2.4. Characterization

2.4.1. Field emission scanning electron microscopy (FE-SEM) and energy dispersive spectrometer (EDS)

The morphologies and the elementary composition of the pure HNTs, PANI/HNTs nanostructures and the AuNPs/PANI/HNTs nanostructures were recorded by a field emission scanning electron microscope (FE-SEM, JEOL ULTRA-55), attaching with an energy dispersive spectrometer (EDS).

2.4.2. Transmission electron microscopy (TEM)

For TEM imaging, the synthesized samples were dispersed in ethanol and drop cast onto the ultra-thin carbon-coated copper grid and dried under infrared lamp for ten minutes, respectively.

2.4.3. Fourier transform infrared spectroscopy (FTIR)

A Thermo Scientific Nicolet 5700 FTIR spectrometer was employed to characterize the FTIR spectra of pure HNTs, PANI/HNTs nanostructures and the AuNPs/PANI/HNTs nanostructures during the wave number of 500–4000 cm^{-1} under ambient conditions.

2.4.4. X-ray diffraction (XRD)

The crystal phase of the acquired samples were checked by a X-ray diffractometer (XRD, Thermo ARL X'TRA) using a Cu Kα radiation source at 35 kV, with a scan rate of 0.02° 2θ s^{-1} in the 2θ range of 10–90°.

2.4.5. X-ray photoelectron spectroscopy (XPS)

The X-ray photoelectron spectra of the obtained examples were testified with an X-ray photoelectron spectrometer (K-Alpha, USA) with Al K X-ray source (1486.6 eV). The high-resolution survey (pass energy = 48 eV) was performed at spectral regions relating to oxygen, nitrogen, gold and sulfur.

3. Results and discussion

Fig. 1 displays the systematic sketch of the fabrication process of AuNPs/PANI/HNTs nanostructures and the obtained FE-SEM images of the obtained samples. As shown in Fig. 1(B1 and B2), the FE-SEM images of naturally occurring HNTs is in the micrometer range, and presents cylinder-shaped and polydisperse. After the *in situ* polymerization of aniline in the suspensions of HNTs, it is clearly that the vast majority of HNTs were coated with PANI (in Fig. 1(D1 and D2)). Fig. 1(F1) illustrated the structures and morphologies of the AuNPs/PANI/HNTs nanostructures, and it is difficult to make the AuNPs out in this magnification. However, from the EDS spectrum, as observed in Fig. 1(F2), the existence of the Au element further demonstrated the successful immobilization of AuNPs on the PANI/HNTs nanostructures.

TEM imaging was used to further determine the detailed microstructure of the samples. As shown in Fig. 2(A and B), the HNTs are about 70 nm in diameter and present obvious hollow structure. After the *in situ* polymerization of aniline, it can be seen in Fig. 2(C and D) that a bundle of HNTs were coated and bounded by short fibrous PANI, as well as the PANI/HNTs nanostructures showed well-dispersion. Along the length direction of the HNTs, most parts of the surface are tightly coated by PANI, and almost no parts of the HNTs are naked, implying the strong binding between HNTs and PANI. There is no obvious change in size and morphology of the PANI nanofibers after the loading of AuNPs on them, and large amounts of AuNPs in uniform and small size are detected in Fig. 2(E and F). Herein, the nitrogens along the polyaniline chain provide physical stabilization for the autoreduced AuNPs, and thiol groups (—SH) can also function as stabilizers for the synthesis of small, stable, monodisperse AuNPs [15,16], which will be further conformed by the XPS analysis.

The structure and composition of the AuNPs/PANI/HNTs nanostructures were further explored by spectroscopy measurement. In the FTIR characterization, as described in Fig. 3(A and a), the characteristic peaks of HNTs that observed at 1630 cm^{-1}, 3621 cm^{-1} and 3696 cm^{-1} are attributed to the deformation of water, O—H stretching of inner hydroxyl groups and O—H stretching of inner-surface hydroxyl groups, respectively. The obvious absorption peaks emerged at 1106 cm^{-1} and 1029 cm^{-1} are in accordance with the in-plane stretching of Si—O [17,18]. On the other hand, it cannot be ignored that there is a significant shift of the two peaks of Si—O, which also implies the successful polymerization of aniline and the reduction of Au ions. The new peaks detected at 1301 cm^{-1}, 1486 cm^{-1}, and 1562 cm^{-1} in Fig. 3(A and b) are ascribed to the vibration of C—C, C=C, and C=N, respectively. Obviously, the intensity of the peaks in Fig. 3(A and c), when compared with that in Fig. 3(A and b) and (A and c), became relatively weak, indicating the strong interaction between $HAuCl_4$ and PANI during the synthesis of AuNPs. It is evident that the strong absorption peak around 1697 cm^{-1} is the characteristic peak of C=O in TA.

The PANI loaded on the HNTs could be further confirmed by XRD. According to the literature, all of the detected peaks can be indexed to the characteristic peaks of HNTs, as primarily shown in Fig. 3(B and a) and (B and b). After the loading of PANI and the formation of AuNPs, it can be seen that the diffraction peaks of HNTs were difficult to observe. At the same time, in the case of AuNPs/PANI/HNTs nanostructures, two new peaks centered at $2\theta = 20.1°$ and 25.2° are the characteristic Bragg diffraction peaks of PANI, suggesting that they have partly crystalline structures, according to previous reports [19,20]. It is also noteworthy that four broad peaks centered at $2\theta = 38.1°$, 44.4°, 64.6° and 77.6° which were observed in Fig. 3(B and c), matching exactly well with the reference values for the Au (1 1 1), Au (2 0 0), Au (2 2 0) and Au (3 1 1) lattice planes, respectively [21,22]. The above results can demonstrate that the AuNPs/PANI/HNTs nanostructures with fibrous PANI and well-dispersed AuNPs were successfully fabricated.

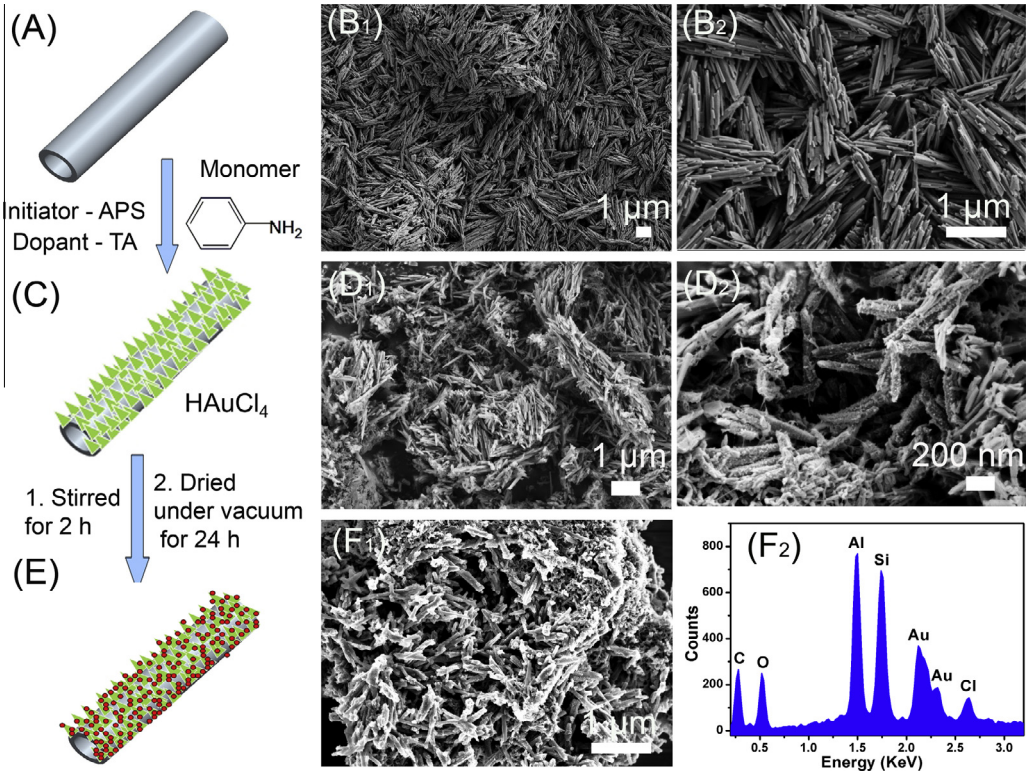

Fig. 1. The schematic illustration of the AuNPs/PANI/HNTs nanostructures (A. HNTs; C. PANI/HNTs; E. the AuNPs/PANI/HNTs nanostructures); the FE-SEM images of the HNTs (B1 and B2), PANI/HNTs (D1 and D2) and AuNPs/PANI/HNTs nanostructures (F1); EDS spectrum of the AuNPs/PANI/HNTs nanostructures (F2).

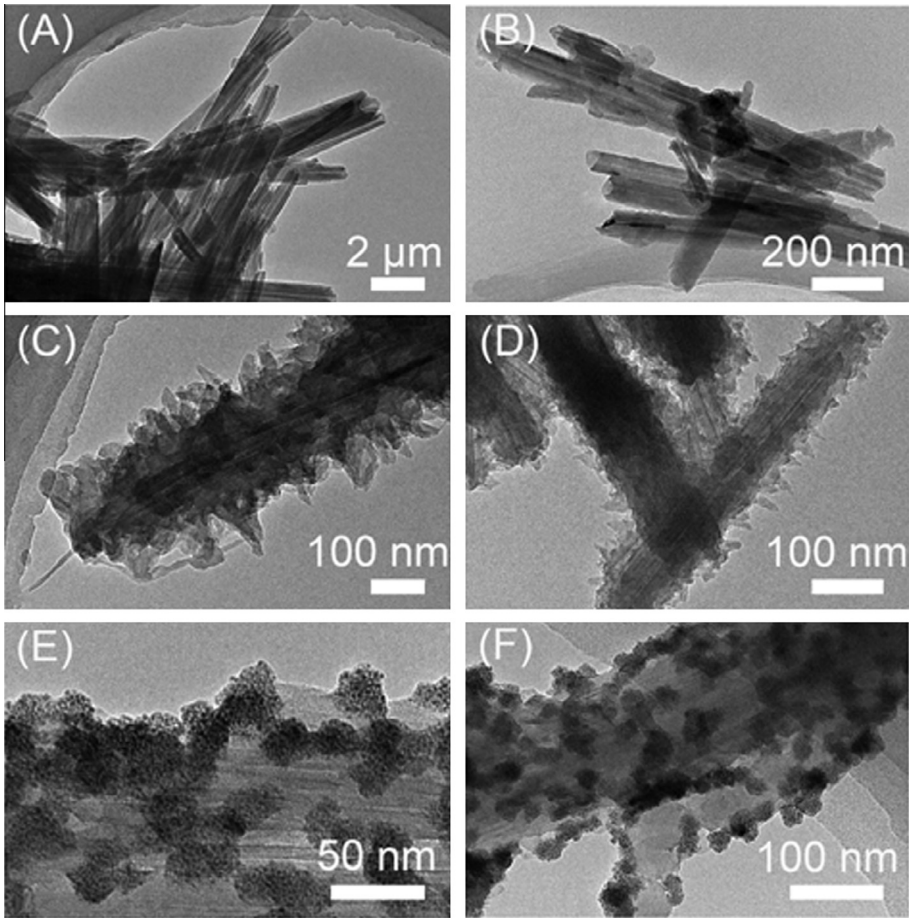

Fig. 2. The TEM images of the HNTs (A and B), PANI/HNTs (C and D) and AuNPs/PANI/HNTs nanostructures (E and F).

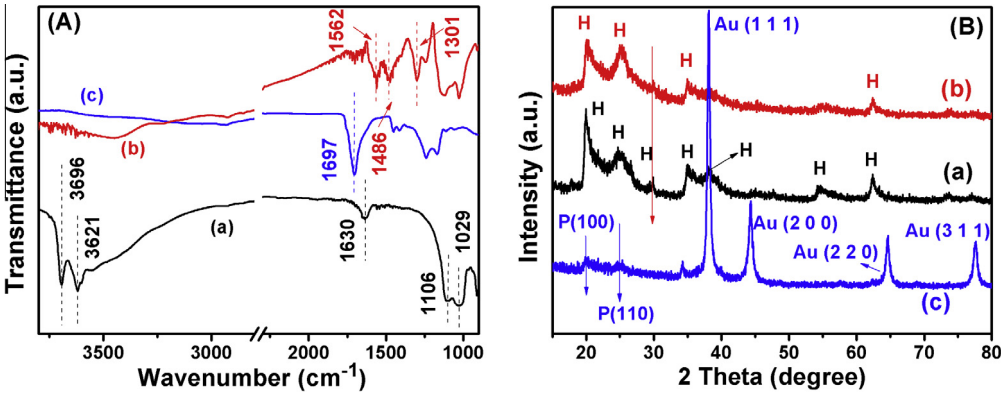

Fig. 3. (A) FTIR spectra and (B) XRD patterns of HNTs (a), PANI/HNTs (b) and AuNPs/PANI/HNTs nanostructures (c). (H: HNTs, P: PANI).

The XPS measurements were used to detect the surface elemental composition and study the chemical process in depth. As depicted in Fig. 4(A), the XPS N 1s spectrum of PANI/HNTs exhibits a peak at 399.2 eV, which is ascribed to the quinonoid imine (=N—) in PANI [23], in the meantime, the other two peaks with binding energy at 399.9 eV and 400.9 eV, which are assigned to the benzenoid amine (—NH—), and positively charged nitrogen (N^+), respectively [24]. After the fabrication of AuNPs/PANI/HNTs nanostructures, the binding energy of the three different states shifts to 399.3, 400.1 and 401.0 eV, which can be observed in Fig. 4(B), respectively. It is apparent that there were significant changes in their relatively intensity between benzenoid amine and quinonoid imine, implying that the benzenoid amine were oxidized to quinonoid imine and it is mainly the nitrogen lone electron pair that interacts with the metal matrix during the redox reaction between PANI and $HAuCl_4$, which were consistent with the theoretical prediction [25]. It can be obviously seen that S 2p spectra have an S 2p3/2, 1/2 doublet structure. The peaks located at 163.7 and 164.8 eV (in Fig. 4(C)) shift to 162.4 and 163.4 eV (in Fig. 4(D)), respectively, which can be attributed to the formation of chemical bond between sulfydryl (—SH) and AuNPs [26]. When the $HAuCl_4$ was dropped into the suspension, the -SH groups could capture Au ions to form SH—Au chelating complex first, and then the SH—Au chelating complex were reduced to Au atoms

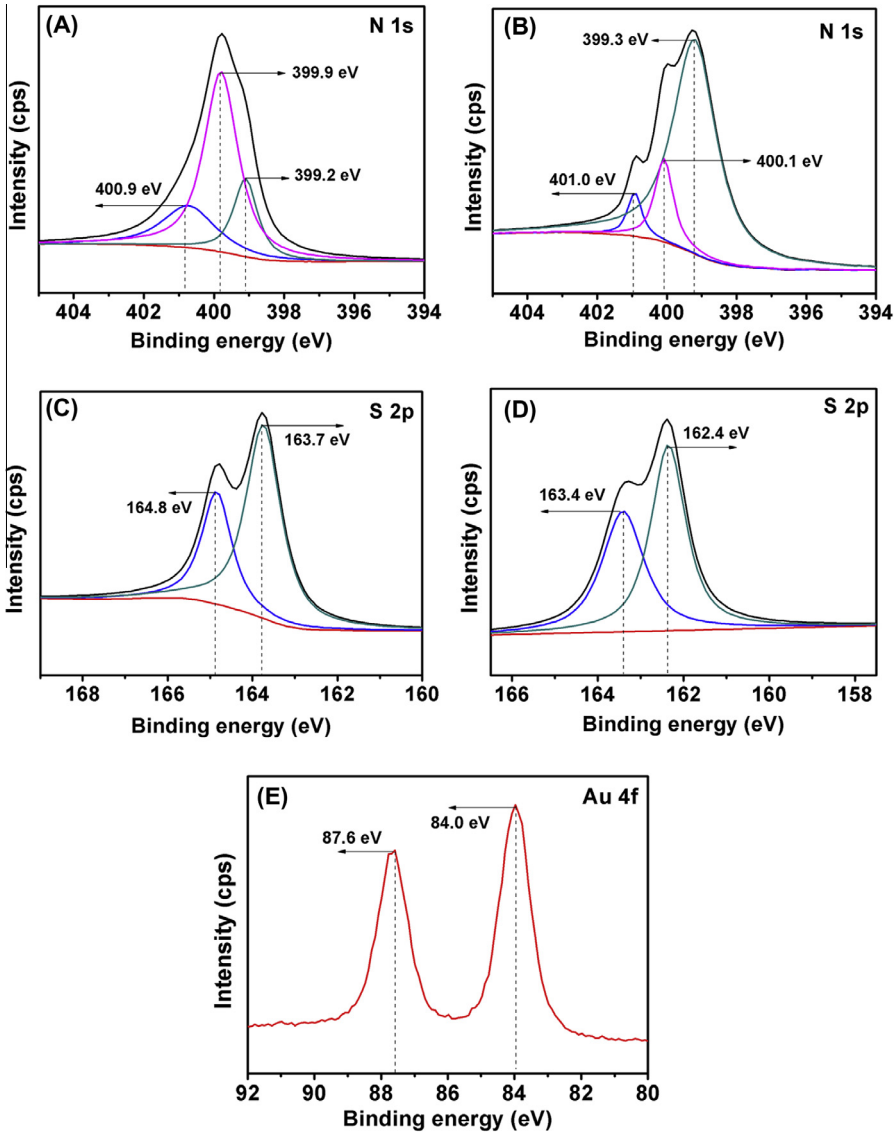

Fig. 4. XPS spectra of N 1s in (A) PANI/HNTs and (B) AuNPs/PANI/HNTs nanostructures, S 2p in (C) PANI/HNTs and (D) AuNPs/PANI/HNTs nanostructures, Au 4f in AuNPs/PANI/HNTs nanostructures (E).

nuclei and grow into nanoparticles gradually, avoiding the aggregation of AuNPs. Yang et al. [27] reported that lower electronegativity and the decrease of binding energy of S 2p would happen when the sulfur attached to metal. As observed in Fig. 4(E), the Au 4f XPS spectrum of Au/PANI/HNTs nanostructures located at 84.0 eV and 87.6 eV correspond well to the standard binding energy of Au° (84.0 and 87.6 eV), which suggests that large quantities of Au ions were reduced to AuNPs. Meanwhile, the binding energy at 87.6 eV implied that there were strong interactions between the small portion of AuNPs and the Au/PANI/HNTs nanostructures [28,29]. Depended on the aforementioned analysis, we can draw conclusions that the AuNPs could be achieved through direct reduction of $HAuCl_4$ by PANI and the TA plays a crucial role in the process of obtaining stable, small and well-dispersed AuNPs [30,31].

As described above, we have fabricated the nanostructured AuNPs/PANI/HNTs composites through a facile route. Considering the good mechanical stability of HNTs and the excellent electrochemical activity of AuNPs and PANI, we hold the view that the AuNPs/PANI/HNTs nanocomposites can be exploited as remarkable electrochemical sensors for the detection of H_2O_2. A 0.1 M phosphate buffer at pH 6.8 was used as a probe to investigate performance of the fabricated H_2O_2 electrode. HRP was employed for the determination of H_2O_2, and HQ was used to detect H_2O_2 as an excellent electron mediator.

For the experiments, cyclic voltammetry (CV) was used to study the electrochemical signal transduction ability of the nanocomposites. The pure HNTs and the blank GCE were used as references in Fig. 5(A and B). Well-defined CV curves were observed in H_2O_2-sensing based on the HRP/(AuNPs/PANI/HNTs)/GCE. The redox peak currents of HQ are about 150 and 30 μA and potentials at −0.3 and 0.45 V, respectively, as depicted in Fig. 5(A and c). On the other hand, as for the HRP/(AuNPs/PANI/HNTs)/GCE, the reduction current (110 μA) caused by HQ decreased to some extent accompanying with the disappearance of the oxidation current peak with the addition of 5.0 mM H_2O_2 in Fig. 5(B and c), implying the existence of strong reactions among HQ, H_2O_2, and HRP [32]. The large distinguishable response toward the detection of H_2O_2 indicates that the charge transport within the AuNPs/PANI/HNTs nanocomposites is relatively fast, indicative of their remarkable electrochemical activity. At the same time, it should be noted that the pure HNTs exhibited relatively poor electrochemical activity in

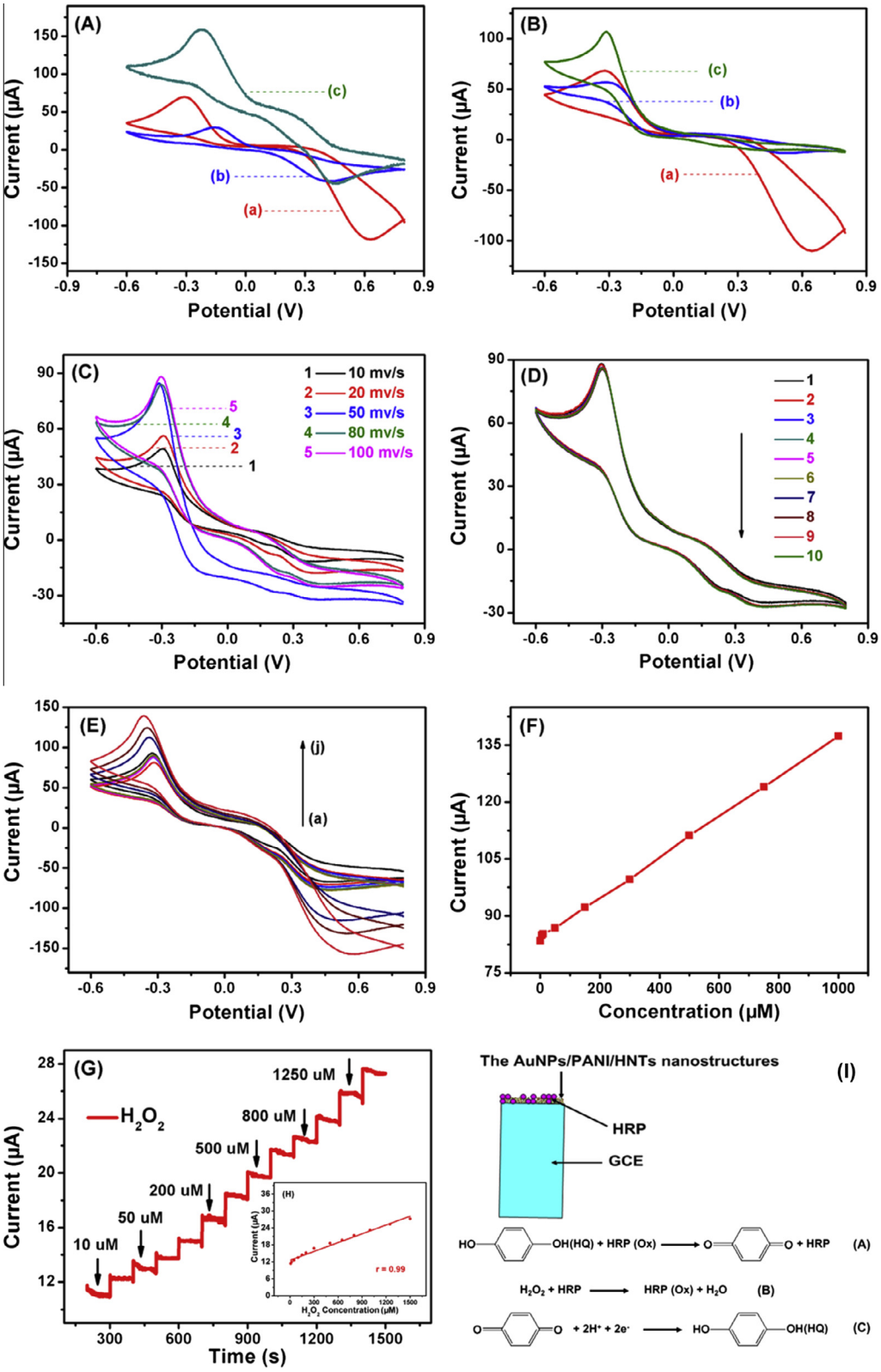

Fig. 5. (A) (In the absence of H_2O_2) and (B) (in the presence of 5.0 mM H_2O_2) are the cyclic voltammograms (CVs) of the blank GCE (a), HRP/pure HNTs/GCE (b) and HRP/(AuNPs/PANI/HNTs)/GCE (c) immersed in 10.0 mM HQ in 0.1 M PBS (pH = 6.8), respectively; (C) the CVs of HRP/(AuNPs/PANI/HNTs)/GCE in the presence of 5.0 mM H_2O_2 in the same conditions at different scan rates; (D) The CVs cycles of HRP/(AuNPs/PANI/HNTs)/GCE in the presence of 5.0 mM H_2O_2 in the same conditions at the scan rate of 100 mV/s; (E) the CVs of HRP/(AuNPs/PANI/HNTs)/GCE in the presence of different concentrations of H_2O_2 (1, 5, 10, 50, 300, 500, 750 and 1000 μM) at the scan rate of 100 mV/s; (F) the reduction peak currents in CV versus H_2O_2 concentration; (G) amperometric response of the fabricated HRP/(AuNPs/PANI/HNTs)/GCE to successive addition of different concentrations of H_2O_2 to 0.1 M PBS; (H) the relationship between the current and the H_2O_2 concentration; (I) schematic presentation of the H_2O_2 sensor based on the HRP/(AuNPs/PANI/HNTs)/GCE and reaction process.

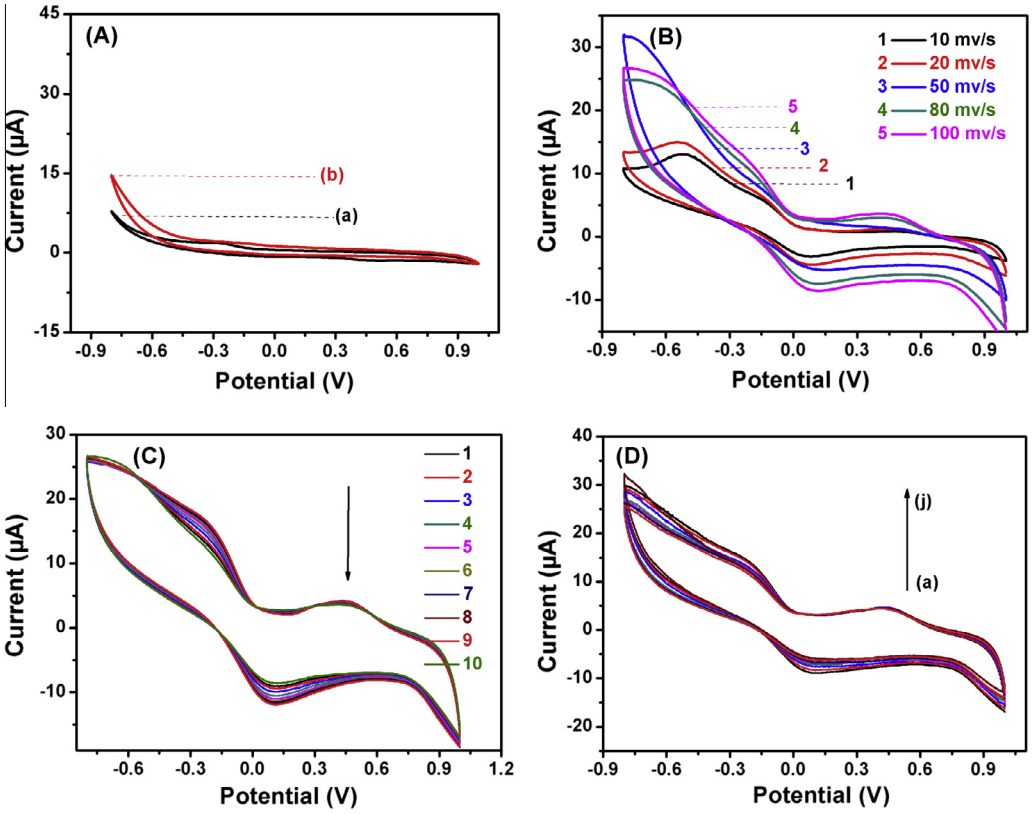

Fig. 6. (A) The cyclic voltammograms (CVs) of the blank GCE (a), and pure HNTs/GCE (b) immersed in 10.0 mM potassium ferricyanide in 0.1 M PBS (pH = 6.8) in the presence of 5.0 mM glucose, respectively; (B) the CVs of (AuNPs/PANI/HNTs)/GCE in the same conditions at different scan rates; (C) the CVs cycles of (AuNPs/PANI/HNTs)/GCE in the same conditions at the scan rate of 100 mV/s; (D) the CVs of (AuNPs/PANI/HNTs)/GCE in the presence of different concentrations of glucose (1, 5, 20, 50, 100, 200, 300, 500, 750, and 1000 μM) at the scan rate of 100 mV/s.

this potential range, as well as the blank GCE showed almost no sensitivity towards H_2O_2, when compared to the HRP/(AuNPs/PANI/HNTs)/GCE, which excluded the interferences effectively. In Fig. 5(C), with the change of the scan rates, the HRP/(AuNPs/PANI/HNTs)/GCE also showed corresponding response, and these phenomena indicated the AuNPs/PANI/HNTs had a good adaptability. As illustrated in Fig. 5(D), the CVs were almost the same and did not shown distinct change. From these facts, we could draw the conclusion that the AuNPs/PANI/HNTs nanocomposites revealed good mechanical stability and reusability and the samples can be acted as excellent electrode material and the HNTs are also employed as reliable supports.

Fig. 5(E and F) shows the electrochemical responses of different concentrations of H_2O_2 solution using HRP/(AuNPs/PANI/HNTs)/GCE as an electrode. It can be observed that an occurrence of reduction current is clearly observed at each period of H_2O_2 injection from 1 μM to 1000 μM at a scan rate of 100 mV/s. We also measured the amperometric response for the HRP/(AuNPs/PANI/HNTs)/GCE to monitor the operational stability and sensitivity of the corresponding electrochemical sensors in the presence of different concentrations of H_2O_2. In Fig. 5(G), stepped increases of the amperometric reduction currents were observed with the addition of H_2O_2. The current response of the sensors was rapidly enhanced and then reached its steady state current, which due to the fast diffusion ratio of the H_2O_2 into the nanostructured AuNPs/PANI/HNTs composites [33–37]. Fig. 5(H) shows a linear relationship with the concentration of H_2O_2 (0.01–1.5 mM) with the correlation coefficient of 0.99, and the detection limit is 0.972 μM at a signal-to-noise ratio of 3.

In addition, we also investigated glucose as model compounds in our experiments to testify the electrochemical activity and flexibility of the sensor. Ramanaviciene et al. [38,39] have already studied glucose biosensor based on polyaniline and AuNPs in the presence of glucose oxidase (GOx) comprehensively. Compared to their research, our study was conducted without the existence of GOx. Fig. 6 showed the CVs of glucose using AuNPs/PANI/HNTs nanocomposites as the working electrode, it is obvious that there were weak redox peaks and successive additions of glucose lead to an increase of the current, suggesting the flexibility and reliability of the AuNPs/PANI/HNTs nanocomposites when acted as electrochemical sensors. Apart from H_2O_2 and glucose, we also anticipated that the prepared nanocomposites could be used to detect glutathione (GSH), ascorbic acid and so forth [40–42].

4. Conclusion

In summary, AuNPs/PANI/HNTs nanostructures had been successfully fabricated through the combination of the *in situ* polymerization of aniline and the facile reduction process of Au ions. The FE-SEM and TEM images demonstrated that the PANI nanofibers were immobilized on the surface of HNTs and great amounts of AuNPs in well-dispersion were implanted into the PANI nanofibers. Further characterizations indicated that the doped PANI nanofibers were preferable reducing agents and stabilizer in the fabrication of AuNPs. Our further experimental results also revealed that the acquired nanostructured AuNPs/PANI/HNTs composites can be acted as reliable electrochemical sensors and exhibited high-sensitivity and well-durability towards the detection of H_2O_2, as well as made further exploration and outlook of its wide applications. Finally, we believe that this type of high-performance nanostructured sensors, combined with a low-cost and

scalable technique shows great potential for use in applications relating to environmental monitoring, beverage industry, and the medical diagnosis.

Acknowledgements

We acknowledge the support of the project of the National Natural Science Foundation of China (NSFC) (51373154), the 521 Talent Project of Zhejiang Sci-Tech University.

References

[1] D.Y. Zhai, B.R. Liu, Y. Shi, L.J. Pan, Y.Q. Wang, W.B. Li, R. Zhang, G.H. Yu, ACS Nano. **7** (2013) 4.
[2] C. Dhand, M. Das, M. Datta, B.D. Malhotra, Biosens. Bioelectron. 26 (2011) 6.
[3] A. Kausaite-Minkstimiene, V. Mazeiko, A. Ramanaviciene, A. Ramanavicius, Biosens. Bioelectron. 26 (2010) 12.
[4] X.C. Tan, J.L. Zhang, S.W. Tan, D.D. Zhao, Z.W. Huang, Y. Mi, Z.Y. Huang, Sensors 9 (2009) 8.
[5] H. Zhu, M.L. Du, M. Zhang, P. Wang, S.Y. Bao, L.N. Wang, Y.Q. Fu, J.M. Yao, Biosens. Bioelectron. 49 (2013) 54.
[6] X.M. Feng, R.M. Li, Y.W. Ma, R.F. Chen, N.E. Shi, Q.L. Fan, W. Huang, Adv. Funct. Mater. 21 (2011) 15.
[7] Y.F. Lin, C.H. Chen, W.J. Xie, S.H. Yang, C.S. Hsu, M.T. Lin, W.B. Jian, ACS Nano. 5 (2011) 2.
[8] C.O. Baker, B. Shedd, P.C. Innis, P.G. Whitten, G.M. Spinks, G.G. Wallace, R.B. Kaner, Adv. Mater. 20 (2008) 1.
[9] Z.C. Xu, Y.L. Hou, S.H. Sun, J. Am. Chem. Soc. 129 (2007) 28.
[10] A. Kumar, L. Joshi, R. Prakash, Ind. Eng. Chem. Res. 52 (2013) 27.
[11] L. Wang, J.L. Chen, L. Ge, Z.H. Zhu, V. Rudolph, Energy Fuels 25 (2011) 8.
[12] Y.M. Lvov, D.G. Shchukin, H. Mohwald, R.R. Price, ACS Nano. 2 (2008) 5.
[13] M.L. Du, B.C. Guo, M.X. Liu, X.J. Cai, D.M. Jia, Phys. B: Condens. Matter. 405 (2010) 2.
[14] X. Zhang, H. Wang, B.Q. Xu, J. Phys. Chem. B 109 (2005) 19.
[15] O.B. Christina, S. Brian, J.T. Ricky, A.M.-M. Alfredo, S.O. Cengiz, O. Mihri, Y. Yang, B.K. Richard, ACS Nano. 5 (2011) 5.
[16] R.J. Tseng, J. Huang, J. Ouyang, R.B. Kaner, Y. Yang, Nano Lett. 5 (2005) 6.
[17] R.J. Wang, G.H. Jiang, Y.W. Ding, Y. Wang, X.K. Sun, X.H. Wang, W.X. Chen, ACS Appl. Mater. Interfaces 3 (2011) 10.
[18] H. Zhu, M.L. Du, M.L. Zou, C.S. Xu, Y.Q. Fu, Dalton Trans. 41 (2012) 34.
[19] H.W. Park, T. Kim, J.J. Huh, M.J. Kang, J.E. Lee, H. Yoon, ACS Nano. 6 (2012) 9.
[20] J.J. Xu, K. Wang, S.Z. Zu, B.H. Han, Z.X. Wei, ACS Nano. 4 (2010) 9.
[21] M.N. Nadagouda, G. Hoag, J. Collins, R.S. Varma, Cryst. Growth Des. 9 (2009) 11.
[22] I. Gorelikov, N. Matsuura, Nano Lett. 8 (2008) 1.
[23] J.R. Pels, F. Kapteijn, J.A. Moulijn, Q. Zhu, K.A. Thomas, Carbon 33 (2005) 11.
[24] R. Ohta, K.H. Lee, N. Saito, Y. Inoue, H. Sugimura, O. Takai, Thin Solid Films 434 (2003) 1.
[25] G. Nesher, G. Marom, D. Avnir, Chem. Mater. 20 (2008) 13.
[26] P. Wang, H. Zhu, S.Y. Bao, M.L. Du, M. Zhang, J. Phys. D: Appl. Phys. 46 (2013) 34.
[27] D.Q. Yang, B. Hennequin, E. Sacher, Chem. Mater. 18 (2006) 21.
[28] Y. Negishi, K. Nobusada, T. Tsukuda, J. Am. Chem. Soc. 127 (2005) 14.
[29] J.A. Larsson, M. Nolan, J.C. Greer, J. Phys. Chem. B 106 (2002) 23.
[30] H. Zhu, M.L. Du, D.L. Yu, Y. Wang, L.N. Wang, M.L. Zou, M. Zhang, Y.Q. Fu, J. Mater. Chem. A 1 (2013) 3.
[31] Y. Jin, H.Y. Chen, M.H. Chen, N. Liu, Q.W. Li, ACS Appl. Mater. Interfaces 5 (2013) 8.
[32] J. Wang, H.B. Yao, D. He, C.L. Zhang, S.H. Yu, ACS Appl. Mater. Interfaces 4 (2012) 4.
[33] Q. Yao, L.D. Chen, W.Q. Zhang, H.C. Liufu, X.H. Chen, ACS Nano. 4 (2010) 4.
[34] M.N. Hyder, S.W. Lee, F.C. Cebeci, D.J. Schmidt, Y. Shao-Horn, P.T. Hammond, ACS Nano. 5 (2011) 11.
[35] W. Pan, X.K. Zhang, H.Y. Ma, J.T. Zhang, J. Phys. Chem. C 112 (2008) 7.
[36] X.Y. Lang, H. Guo, L.Y. Chen, A. Kudo, J.S. Yu, W. Zhang, A. Inoue, M.W. Chen, J. Phys. Chem. C 114 (2010) 6.
[37] S.P. Zhou, H.M. Zhang, X.H. Wang, J. Li, F.S. Wang, RSC Adv. 3 (2013) 6.
[38] N. German, A. Ramanavicius, J. Voronovic, A. Ramanaviciene, Colloids and Surf. A: Physicochem. Eng. Aspects 413 (2012) 5.
[39] V. Mazeiko, A. Kausaite-Minkstimiene, A. Ramanaviciene, Z. Balevicius, A. Ramanavicius, Sens. Actuators B: Chem. 189 (2013).
[40] A. Kausaite-Minkstimiene, V. Mazeiko, A. Ramanaviciene, A. Ramanavicius, Sens. Actuators B: Chem. 158 (2011).
[41] F. Chai, C. Wang, T. Wang, L. Li, Z.M. Su, ACS Appl. Mater. Interfaces 2 (2010) 5.
[42] Y.Y. Liu, Q.X. Zhou, Z.H. Zeng, R. Qiao, X.S. Wang, B.W. Zhang, J. Phys. Chem. B 112 (2008) 32.